Experimental Eye Research 209 (2021) 108646

Contents lists available at ScienceDirect

Experimental Eye Research

journal homepage: www.elsevier.com/locate/yexer

Spatiotemporal determination of metabolite activities in the corneal epithelium on a chip

Rodi Abdalkader [a,1,**], Romanas Chaleckis [b,c], Craig E. Wheelock [b,c], Ken-ichiro Kamei [a,d,*]

[a] Institute for Integrated Cell-Material Sciences (WPI-iCeMS), Kyoto University, Yoshida-Ushinomiya-cho, Sakyo-ku, Kyoto, 606-8501, Japan
[b] Gunma University Initiative for Advanced Research (GIAR), Gunma University, Maebashi, Gunma, 371-8511, Japan
[c] Division of Physiological Chemistry 2, Department of Medical Biochemistry and Biophysics, Karolinska Institute, Stockholm, 171-77, Sweden
[d] Wuya College of Innovation, Shenyang Pharmaceutical University, Liaoning, 110016, PR China

ARTICLE INFO

Keywords:
Corneal epithelium on a chip
Untargeted metabolomics
Metabolism
Transporters

ABSTRACT

The corneal epithelial barrier maintains the metabolic activities of the ocular surface by regulating membrane transporters and metabolic enzymes responsible for the homeostasis of the eye as well as the pharmacokinetic behavior of drugs. Despite its importance, no established biomimetic in vitro methods are available to perform the spatiotemporal investigation of metabolism and determine the transportation of endogenous and exogenous molecules across the corneal epithelium barrier. This study introduces multiple corneal epitheliums on a chip namely, Corneal Epithelium on a Chip (CEpOC), which enables the spatiotemporal collection as well as analysis of micro-scaled extracellular metabolites from both the apical and basolateral sides of the barriers. Longitudinal samples collected during 48 h period were analyzed using untargeted liquid chromatography–mass spectrometry metabolomics method, and 104 metabolites were annotated. We observed the spatiotemporal secretion of biologically relevant metabolites (i.e., antioxidant, glutathione and uric acid) as well as the depletion of essential nutrients such as amino acids and vitamins mimicking the in vivo molecules trafficking across the human corneal epithelium. Through the shifts of extracellular metabolites and quantitative analysis of mRNA associated with transporters, we were able to investigate the secretion and transportation activities across the polarized barrier in a correlation with the expression of corneal transporters. Thus, CEpOC can provide a non-invasive, simple, yet effectively informative method to determine pharmacokinetics and pharmacodynamics as well as to discover novel biomarkers for drug toxicological and safety tests as advanced experimental model of the human corneal epithelium.

1. Introduction

The corneal epithelial barrier is the main structure that determines the pharmacokinetics and pharmacodynamics of drugs into the interior segment of the eye and contributes to the maintenance of homeostasis of the ocular surface by controlling the metabolism and transportation of different molecules from and to the tear pool (Nirmal et al., 2013; Xiang et al., 2009). Nutrients and drugs are actively or passively transported through the corneal epithelial barrier, followed by their intracellular metabolism, modification, and secretion of the corresponding metabolites. Although many metabolic pathways (e.g., oxidative, hydrolytic, reductive, and conjugative pathways) (Argikar et al., 2017; Čejková et al., 2004) and transporters (Kölln and Reichl, 2012; Zhang et al., 2008) in the cornea have been investigated, the spatiotemporal mechanisms of the in situ metabolism and transportation of drugs through the human corneal epithelial barrier are barely known, owing to the technical difficulties in the current corneal experimental platforms as well as the lack of analytical tools that non-invasively enable longitudinal metabolome monitoring in small volumes (Larrea et al., 2007; Rönkkö et al., 2016). Moreover, while the current in vitro corneal models that use cell-culture inserts (e.g., a transwell system) have been investigated, they only provide a two-dimensional structure of the corneal epithelial

* Corresponding author. Institute for Integrated Cell-Material Sciences (WPI-iCeMS), Kyoto University, Yoshida-Ushinomiya-cho, Sakyo-ku, Kyoto, 606-8501, Japan.
** Corresponding author.
E-mail addresses: rodi@fc.ritsumei.ac.jp (R. Abdalkader), kamei.kenichiro.7r@kyoto-u.ac.jp (K.-i. Kamei).
[1] Current affiliation: Ritsumeikan Global-Innovation Research Organization (R-GIRO), Ritsumeikan University; 1–1–1 Nojihigashi, Kusatsu, Shiga 525–8577, Japan.

https://doi.org/10.1016/j.exer.2021.108646
Received 3 April 2021; Received in revised form 10 May 2021; Accepted 27 May 2021
Available online 5 June 2021

cells, which is physiologically different that in the cornea (Hornof et al., 2005; Reichl, 2008). Therefore, in vitro biomimetic models of the cornea need to be established. These aforementioned requirements can be fulfilled by identifying an alternative in vitro platform that can simulate the structure of the corneal epithelial barrier. Unlike classical models, organ-on-a-chip (OoC) technology is a promising approach for the recreation of miniaturized organs in micro-scaled devices (Huh et al., 2010), because it can provide proper three-dimensional extracellular environments as well as dynamic flow and mechanical stimuli (Abdalkader and Kamei, 2020; Bennet et al., 2018; Bhatia and Ingber, 2014; Seo and Huh, 2014). These OoC advantages allow the elucidation of metabolic and transportation activities in the human corneal epithelial barrier under conditions simulating physical stimuli-mediated by eye-blinking in vitro. We previously developed an OoC platform with multiple corneal epithelial barriers in a single microfluidic device having apical and basolateral sides under eye blinking-like stimuli, and aqueous humor drainage within the device could characterize both the anatomical structure as well as the biomechanical nature of the corneal epithelial barrier (Abdalkader and Kamei, 2020). In addition to the OoC platform, to determine the overall biological function of the corneal epithelial barrier on a chip in a spatiotemporal manner, we need a non-invasive analytical tool that allows the accurate monitoring of enzyme and transporter activities. Many OoC platforms developed to study the metabolism and transport mechanisms use optical or fluorescent assays [e.g., 3-(4,5-dimethylthial-2-yl)-2,5-diphenyltetrazalium bromide (MTT)] and lucifer yellow (Bovard et al., 2018; Jang et al., 2019; McAleer et al., 2019). However, these assays provide very limited information that is restricted to a single target and might cause cellular damage because of the use of additional chemical compounds. In addition to optical and fluorescent assays, untargeted metabolomic analysis based on liquid chromatography–mass spectrometry (LC-MS) is a preferred methodology, since it allows quantification of numerous metabolites in a single measurement (Sévin et al., 2017; Theodoridis et al., 2013). Moreover, we have developed an LC-MS-based untargeted metabolomics workflow enabling non-invasive temporal quantification of micro-scaled extracellular metabolites (Abdalkader et al., 2020). Thus, the OoC platform in combination with LC-MS untargeted metabolomics might provide deeper insights into the metabolic and transport activities of the improved human corneal epithelial barrier than those provided by conventional cell culture and assay platforms.

Herein, we introduce our OoC platform to reconstruct the human corneal epithelium, namely, corneal epithelium on a chip (CEpOC), for the spatiotemporal collection and analysis of extracellular metabolite secretion and transportation across the barrier. The CEpOC allows the collection of extracellular metabolites separately at the apical and basolateral sides of corneal epithelial cells. Quantitative real time-polymerase chain reaction (RT-PCR) analysis can then be used to evaluate the expression levels of transporters in the corneal epithelial cells. To our knowledge, this is the first study to show that the integration of CEpOC and untargeted metabolomics can allow the assessment of the activities, secretion, and transportation of metabolites across the corneal epithelial barrier.

2. Materials and methods

2.1. Microfluidic device fabrication

The microfluidic device was fabricated using stereolithographic 3D-printing techniques and solution cast-molding processes (Abdalkader and Kamei, 2020; Kamei et al., 2015). In brief, the mold for microfluidic channels was produced using a 3D printer (Keyence Corporation, Osaka, Japan). Two molds were fabricated: the upper and lower blocks. Each block contained four chambers (15 mm length, 1.5 mm width, and 0.5 mm height). Before use, the surfaces of the molds were coated with trichloro (1H,1H,2H,2H-perfluorooctyl) silane (Sigma-Aldrich, St. Louis, MO, USA). Sylgard 184 PDMS two-part elastomer (ratio of pre-polymer to curing agent, 10:1; Dow Corning Corporation, Midland, MI, USA) was mixed, poured into the molds to produce 4-mm and 0.5-mm thick PDMS upper and lower layers, respectively, and degassed using a vacuum desiccator for 1 h. The PDMS of the lower block was fixed on a glass slide and then cured in an oven at 80 °C for 24 h. After curing, the PDMS was removed from the molds, trimmed, and cleaned. A clear PET membrane (pore size, 0.4 μm; thickness, 10 μm; nominal pore density, 4×10^6 pores cm^{-2}) was fixed on each chamber of the lower PDMS block. Both the PDMS blocks were treated with corona plasma (Shinko Denki, Inc., Osaka, Japan) and bonded together by baking in an oven at 80 °C.

2.2. Human corneal epithelial cell culture

HCE-T cells were provided by RIKEN Bioresource Research Centre (Ibaraki, Japan). Cells were cultured in DMEM/F12 supplemented with 5% (v/v) fetal bovine serum, 5 μg mL^{-1} insulin, 10 ng mL^{-1} human epithelial growth factor, and 0.5% dimethyl sulfoxide. The cells were passaged with trypsin-EDTA (0.25–0.02%) solution at a 1:4 subculture ratio.

2.3. Human corneal epithelial barrier construction in the microfluidic device

Before use, the microfluidic cell culture devices were placed under ultraviolet light in a biosafety cabinet for 30 min. The microfluidic channels were washed with DMEM/F12. Cells were harvested using trypsin and collected in a 15 mL tube. Following centrifugation, the cells were resuspended in DMEM/F12 medium and introduced into the upper channel of the microfluidic devices via a cell inlet with a cross-sectional area of 0.23 cm^2 at a density of 1×10^6 cells mL^{-1}. The lower receiver channel was filled with DMEM/F12 only. The microfluidic devices were then placed in a humidified incubator at 37 °C with 5% CO_2 for 7 days. The medium in each chamber was periodically changed every 24 h.

2.4. Cell viability assay

Cell viability was assessed by live staining with Calcein AM (Dojindo Molecular Technologies, Inc.). In brief, cells were incubated with Calcein AM at a final concentration of 10 μg mL^{-1} in DMEM/F12 medium at 37 °C for 60 min. The cells were then washed twice with PBS and subjected to microscopy imaging.

2.5. Immunofluorescence and microscopy imaging

For immunostaining, cells were fixed with 4% paraformaldehyde in PBS for 25 min at 25 °C and then permeabilized with 0.5% Triton X-100 in PBS for 10 min at 25 °C. Subsequently, the cells were blocked with blocking buffer [5% (v/v) normal goat serum, 5% (v/v) normal donkey serum, 3% (w/v) bovine serum albumin, 0.1% (v/v) Tween-20] at 4 °C for 24 h and then incubated at 4 °C overnight with the primary antibodies in blocking buffer (Table S1). Cells were then incubated at 37 °C for 60 min with a secondary antibody (Alexa Fluor 594 donkey anti-rabbit IgG and Alexa Fluor 594 donkey anti-mouse IgG, 1:1000; Jackson ImmunoResearch, West Grove, PA, USA) in blocking buffer before final incubation with 4,6-diamidino-2-phenylindole (DAPI) or anti-phalloidin for F-actin at 25 °C. For imaging, we used a Nikon ECLIPSE Ti inverted fluorescence microscope equipped with a CFI plan fluor (10 × /0.30 N.A. objective lens; Nikon, Tokyo, Japan). Z-scans were obtained using an Andor Multi-model Fast Confocal Microscope System Dragonfly (Oxford Instruments, Abingdon, UK). Images were then analyzed using ImageJ software (National Institute of Health, Maryland, USA) or CellProfiler software (Version 3.1.8; Broad Institute of Harvard and MIT, USA) (McQuin et al., 2018).

2.6. Quantitative RT-PCR array

Total RNA from microfluidic channels was purified using RNeasy Mini Kit (Qiagen). Next, 0.3 μg of total RNA was reverse-transcribed using the RT First-strand Kit (Qiagen). The cDNA obtained in solution was mixed with Power SYBR Green PCR MasterMix (Life Technologies) and introduced into the Drug Transporter-specific RT2 Array (Qiagen, Cat. no. 330231 PAHS-070ZA) in a 96-well format, according to the manufacturer's instructions. PCR conditions were as follows: initial incubation at 95 °C for 10 min, followed by 40 cycles of 95 °C for 15 s and then 60 °C for 3 min; an Applied Biosystems 7300 Real-Time PCR system (Life Technologies) was used for the PCRs. The mRNA repression was performed using the $2^{-\Delta CT}$ method, where ΔCT = CT (gene of interest; GOI) − CT (housekeeping genes; HKG).

2.7. Extracellular culture medium collection for untargeted metabolomics

After the HCE-T cells were cultured for 7 days, the culture medium was replaced with fresh medium in both the apical and basolateral channels of the microfluidic device. Microfluidic devices were then placed at 37 °C with 5% CO_2. At 0, 6, 12, 24 and 48 h time points, a sample consisting of 1 μL of extracellular culturing medium from both the apical and basolateral channels was collected. The collected samples were dried in a vacuum incubator for 3 h at 25 °C and then preserved at −80 °C.

2.8. Untargeted LC-MS metabolomics

Tubes containing 1 μL of dried sample were thawed and 100 μL of water:acetonitrile (1:9, v/v) mixture containing five technical internal standards (tISs) was added (Table S2). For the preparation of quality control (QC) samples, 0 h cell culture medium sample was used from our previous study (Abdalkader et al., 2020). For each QC sample, 1 μL of cell culture medium was evaporated and resuspended as study samples. After resuspension, all samples were centrifuged at 4 °C for 15 min at 20000 *g*. Next, 40 μL of the supernatant was transferred to a 96-well 0.2 mL PCR plate (PCR-96-MJ; BMBio, Tokyo, Japan). The plate was sealed with a pierceable seal (4titude; Wotton, UK) for 3 s at 180 °C by using a plate sealer (BioRad PX-1; CA, USA) and maintained at 4 °C during the LC-MS measurement. The injection volume was 10 μL. The LC-MS method has been described previously (Chaleckis et al., 2018; Naz et al., 2017; Tada et al., 2019). In brief, metabolite separation was achieved on an Agilent 1290 Infinity II system by using SeQuant ZIC-HILIC (Merck, Darmstadt, Germany) column by using a 12 min gradient of acidified acetonitrile and water. Data were acquired on an Agilent 6550 Q-TOF-MS system with a mass range of 40–1200 m/z in the positive all ion fragmentation mode, including 3 sequential experiments at alternating collision energies: one full scan at 0 eV, followed by one MS/MS scan at 10 eV, and then one MS/MS scan at 30 eV. The data acquisition rate was 6 scans/s. Data were converted to mzML format by using Proteowizard (Chambers et al., 2012) and processed using MS-DIAL version 4.38 (Tsugawa et al., 2015) (detailed parameters are shown in Table S4 and S5). An in-house MS2 spectral library containing experimental MS2 spectra and retention times (RTs) for 391 compounds obtained from standards (Meister et al., 2021; Naz et al., 2017; Tada et al., 2019) was used to annotate the detected compounds on the basis of 3 criteria: (i) accurate mass (AM) match (tolerance: 0.01 Da), (ii) RT match (tolerance: 1 min), and (iii) MS2 spectrum match (similarity, >80%). The MS2 similarity was scored as a simple dot product without any weighting (at least two MS2 peaks matched with the reference spectra). The MS2 similarities with reference spectra were matched to any of the CorrDec (Tada et al., 2020) or MS2Dec (Tsugawa et al., 2015) deconvoluted MS2 spectra of the three collision energies (0, 10, and 30 eV). Peak areas exported from MS-DIAL were used for metabolite semi-quantification. Metabolites with CV of <30% in QC samples or D-ratio (Broadhurst et al., 2018) of <50% were used for further analyses. The dataset has been deposited to the EMBL-EBI MetaboLights repository with the identifier MTBLS2274 (Haug et al., 2020).

2.9. Statistical analysis

All data were analyzed as the mean ± SEM. The unpaired *t*-test and Tukey's comparison test were performed using GraphPad prism 8 (GraphPad Software, La Jolla California, USA). ANOVA post-hoc analysis among metabolites was performed by MetaboAnalyst platform (Chong et al., 2018). Orange 3 software (Version 3.23.1; Bioinformatics Laboratory, Faculty of Computer and Information Science, University of Ljubljana, Slovenia). The biological pathways analysis was performed using the and Reactome Platform (Fabregat et al., 2018).

3. Results

3.1. The construction of CEpOC

To investigate the process of molecular transport, secretion, and metabolism in the corneal epithelial barrier (Fig. 1A), we constructed the CEpOC by using a multi-well microfluidic device (Fig. 1B).

To construct CEpOC, we seeded the HCE-T cells in the upper channels and cultured them under static conditions for 7 days. During the 7-day culture on the chip, HCE-T cells proliferated to cover the entire porous membrane (Fig. S1). Next, to confirm the intactness and polarity of the barrier, we performed qualitative fluorescent immunocytochemistry to analyze the expression of tight junction proteins (zonula occludens protein-1; ZO-1) and F-actin filaments (phalloidin; Fig. 1C). We noticed a clear appearance in ZO-1 and F-actin filaments. Fluorescent immunocytochemistry analysis also revealed that the HCE-T cells cultured on the chip expressed cytokeratin-12 (CK-12, a marker of corneal epithelium maturation) and P-glycoprotein (P-gp, also known as multidrug-resistance protein 1; MDR1, a transmembrane transporter (Fig. 1D).

3.2. Gene profiling of metabolic transporters on human corneal cells

To investigate metabolic and transporting activities in the CEpOC, we evaluated the mRNA expression of 85 well-known transporters by using a qPCR array in HCE-T cells (Fig. 2, and Table S2). We found the expression of a wide range of transporters (threshold of mRNA expression, $2^{-\Delta Ct} \geq 10^{-3}$) mainly among the genes of the superfamily of solute carrier (SLC)-related transporters, including 14 subgroups (SLC2A1/A2/A3, SLC3A2, SLC5A1, SLC7A5/A6/A7/A8/A11, SLC10A1, SLC16A1/A2/A3, SLC19A1/A2, SLC22A1/A2/A9, SLC25A13, SLC28A1/A3, SLC29A1/A2, SLC31A1, SLC38A2/A5, SLCO2A1/SLCO3A1/SLCO4A1, and SLO1B1/SLO2B1) that mediate the transportation of peptides, monocarboxylic acids, nucleosides, organic anions/cations, glucose, and amino acids (Alexander et al., 2015). In addition, the ATP-binding cassette (ABC) transporter family, including 6 major subgroups (ABCA2/A5/A9/A12, ABCB1/B4/B6, ABCC1/C3/C4/C5/C16, ABCD1/D4, ABCF1, and ABCG2) responsible for the transportation and efflux of xenobiotics and endogenous molecules, showed remarkable expression (Rees et al., 2009). The two subfamilies (VDAC1-C2) of voltage-dependent anion channels Transporter 1 (VDACs), ABC transporter sub-family B [MDR/TAP1-2 and major vault protein (MVP)], which mediate the transportation of xenobiotic toxins, were markedly expressed.

3.3. Measurement of extracellular metabolites in the CEpOC

By using our previously developed untargeted LC-MS method for the measurement of extracellular metabolites at the microscale level (Abdalkader et al., 2020), we could annotate 104 metabolites at Metabolomics Standard Initiative annotation level 1 (Sumner et al., 2007). Peak areas were used for metabolite semi-quantification. All tISs

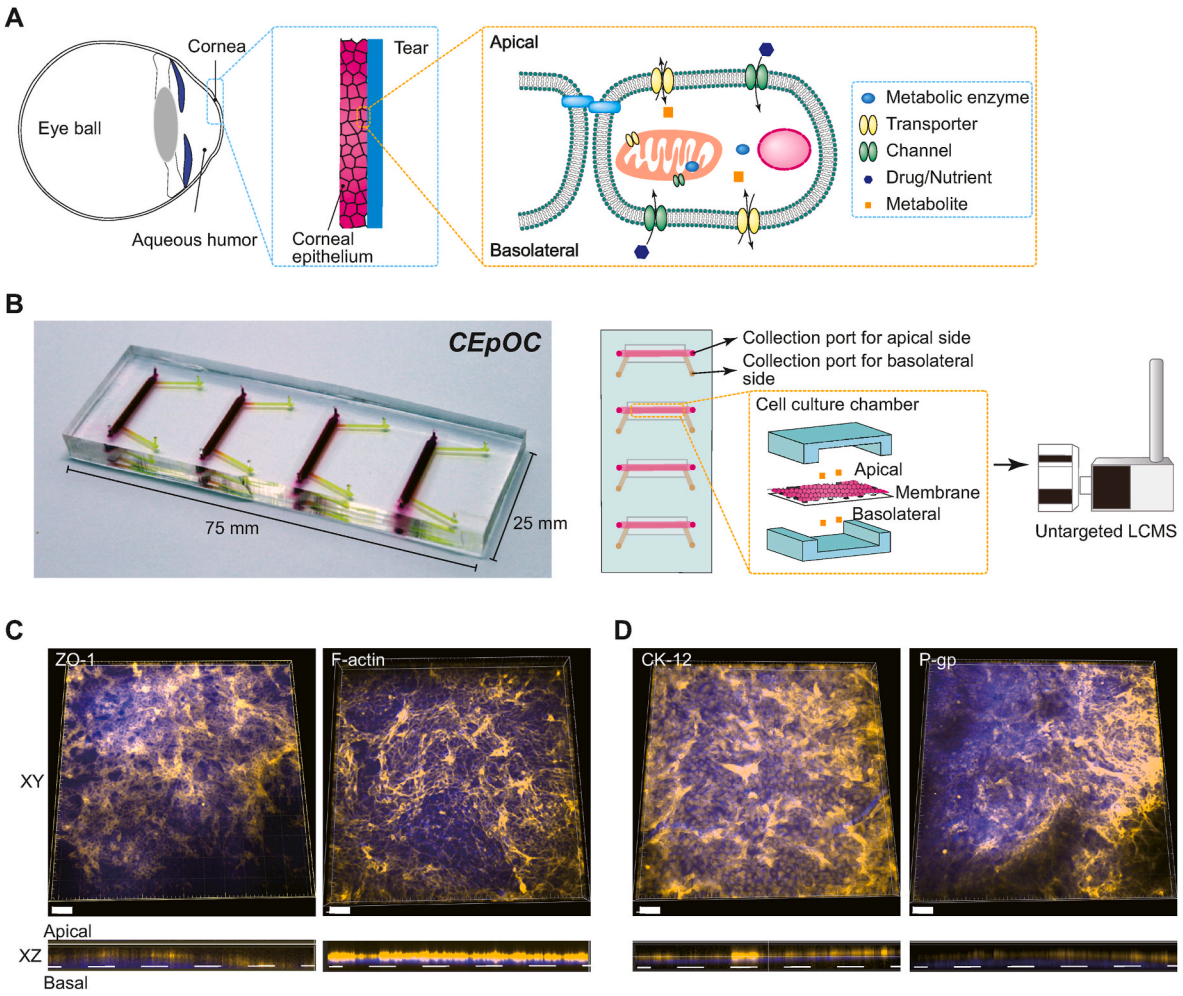

Fig. 1. Multiple corneal epithelial barriers on a chip, namely, CEpOC. (A) An illustration of the overall structure of the ocular surface, and a scope that shows the role of the corneal barrier in the transportation or metabolism of nutrients and drugs. (B) A photograph of Cornea-Chip, and an illustration of its cross-section showing the cell culture chamber from the top to bottom: the upper channel, corneal epithelial cells, porous membrane, and lower channel as well as its applicability for the determination of extracellular metabolites by using untargeted LC-MS instrumentation. Each chamber has sample collection ports for apical and basolateral sides. (C) Immunofluorescence staining indicating the barrier polarity and intactness (ZO-1 and F-actin). (D) Immunofluorescence staining indicating the expression of corneal epithelium maturation marker (CK-12), and the apical ABC-related family of transporter protein (P-gp) expression. XZ dimensions refer to the cross-section scanning images obtained using confocal scanning microscopy. Experimental data are collected from HCE-T cells grown in microfluidic devices for 7 days. Yellow: ZO-1, F-actin, Ck-12, P-gp; blue: DAPI. Scale bar, 100 μm.

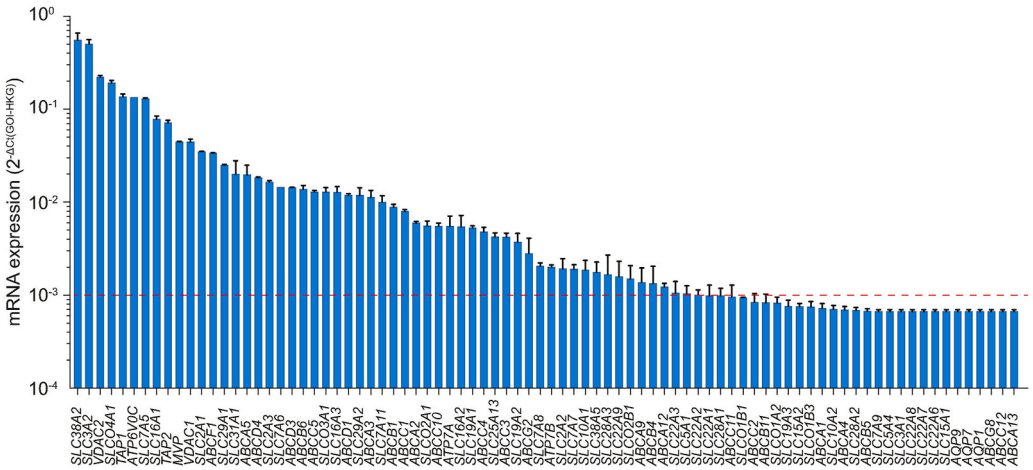

Fig. 2. Quantitative analysis of mRNA expression associated with transporters in the Cornea-Chip. The red dashed line indicates the threshold of mRNA expression. Data are presented as means ± S.E.M. (n = 2).

showed coefficient of variation (CV) of peak areas of ≤17% across the QC samples and <13% in the study samples (except 5-fluorocytosine, 39.7%). The median CV of all detected metabolites was 9.9% in the QC samples. The median CV of all detected metabolites in the triplicate measurements was 16%. In the principal component analysis (PCA), samples were clustered by all groups indicating systematic metabolite shifts in raw peak area values (Fig. S3) as well as in peak area values corrected by the volume of microfluidic channels (Fig. 3D). QCs and study samples were clearly separated with narrow CIs among the triplicates of each sample in stepwise time-dependent alterations of extracellular metabolites from both apical and basolateral sides. Eventually we used Calcein AM staining at the end of extracellular metabolites collection (48 h) to confirm that sample collection did not cause cellular damage. There was no significant change in the mean fluorescence intensity of Calcein AM among the cells at different locations in the microchannels as well as between different cell chambers (Fig. 3B and C).

3.4. Biological pathways and transportation activities

To further explore the corneal metabolic and transporting activities based on the obtained metabolomic profiles, we used the MetaboAnalyst platform (Chong et al., 2018). According to the analysis of variance (ANOVA) post-hoc comparison, all 104 annotated metabolites varied significantly (Fig. S4). By the employment of Reactome platform to investigate biological pathways ($P < 0.05$) (Fabregat et al., 2018), we found that 74 out of the 104 metabolites were associated with the transport of nucleosides and free purine and pyrimidine across the plasma membrane (mostly associated with SLC transmembrane transporters (SLC28 and SLC29) (Alexander et al., 2015)), metabolism-catabolism of nucleotides, purine/pyrimidine catabolism/-transportation, metabolism of amino acids and derivatives, and glutathione synthesis/recycling. Moreover, metabolites showed a significant relationship with a wide range of SLC transporters, including vitamins, organic cation/anion/zwitterion transporters (SLC22) (Lin et al., 2015; Nigam et al., 2015), as well as ABC transporter family members (Rees et al., 2009).

Interestingly we could observe three different patterns of metabolite transport across the barriers based on the criteria of fold difference of apical/basolateral metabolites: Category I (fold difference, ≥2), in which metabolite secretion was observed in the apical sides or in both the apical and basolateral sides. Category II (−2 < fold difference < 2), where metabolites had no notable secretion or clearance in both the apical and basolateral sides. Category III (fold difference, ≥2), in which nutrient metabolites were gradually depleted from both the apical and basolateral sides with respect to their kinetic rates. In Category I, glutathione (GSH), uric acid, 3-ureidopropionic acid, 3-ureidoisobutyric acid, 1-methyl nicotinamide, *N*-acetyl putrescine, folinic acid, uracil, 2-*O*-methylinosine, N^2N^2 dimethyl guanosine, N^1-methyl guanosine, and 7-methylguanine showed significant increase (Fig. 4B and Fig. S5). As for Category II metabolites, a slight depletion or secretion without any distinction in activity between the apical or basolateral sides was observed. In Category III, metabolites such as cysteine-*S*-sulfate, N^6-succinyladenosine, hypoxanthine, creatine, aspartic acid, phenylacetylglutamine, glutaryl-/octenoyl-/propionyl-/oleoyl-/palmitoyl-carnitine, carnitine, taurine, asparagine, N^a-acetyl arginine, adenosine, and other amino acids were gradually depleted from both the apical and basolateral sides, but with different clearance rates (Fig. 4B and Fig. S5C). Metabolite clearance was quicker in the apical side: the depletion rates (K) of cysteine-*S*-sulfate (Fig. 4C), hypoxanthine, and oleoyl-carnitine (Fig. S5C) were 0.23, 0.25, and 0.2 h^{-1}, respectively. In contrast, on the basolateral side, these metabolites showed low K values (0.01, 0.02, and 0.005 h^{-1}, respectively; Fig. 4C and Fig. S5C).

4. Discussion

Corneal metabolic activities have been investigated to an extent to understand the pharmacological outcomes detailing the activation, inactivation, and clearance of xenobiotics as well as endogenous molecules mainly for the purpose of the development of prodrugs (Čejková et al, 2002, 2004). Furthermore, transporters such as solute-linked carriers and adenosine triphosphate binding cassette families (ABC) were found to have an important role in the homeostasis of corneal epithelial barrier (Becker et al., 2007; Dahlin et al., 2013). However, the spatiotemporal determination of metabolites activities, and the in-situ transportation within the corneal barrier is barely elucidated. These kinds of studies

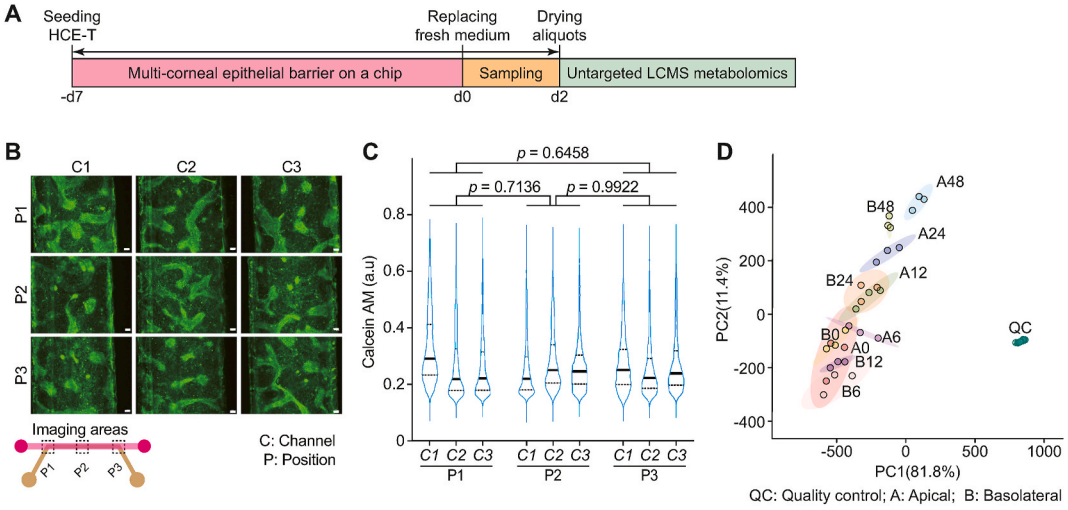

Fig. 3. Spatiotemporal analysis of extracellular metabolites from the corneal epithelial barrier on a chip. (A) The procedure for collecting and processing extracellular metabolites from the multi-corneal barriers on a chip. (B) Cell viability in the microfluidic devices by using Calcein AM staining. HCE-T human corneal epithelial cells in the microfluidic devices at the end of extracellular metabolites collection (48 h). Green, Calcein-AM. Scale bar, 100 μm. (C) Microscopic signal-cell analysis for evaluating cell viability based on calcein-AM staining shown in B. The analysis was performed on images of 3 independent samples; 4300 cells were randomly selected and analyzed for each sample. Data are represented in the violin plot in which the median of each group is indicated with a scatter line (25th to 75th interquartile range). The *p*-values were determined using Tukey's multiple comparison test. D, Principal component analysis (PCA) of metabolomics dataset peak areas corrected by channel volume and transformed into cube root values (Supplementary Fig. 3, data are not corrected by channel volume). The 95% confidence regions are highlighted in different colors. AP: apical, BA: basal, QC: quality controls. Data are derived from 3 biological replicates.

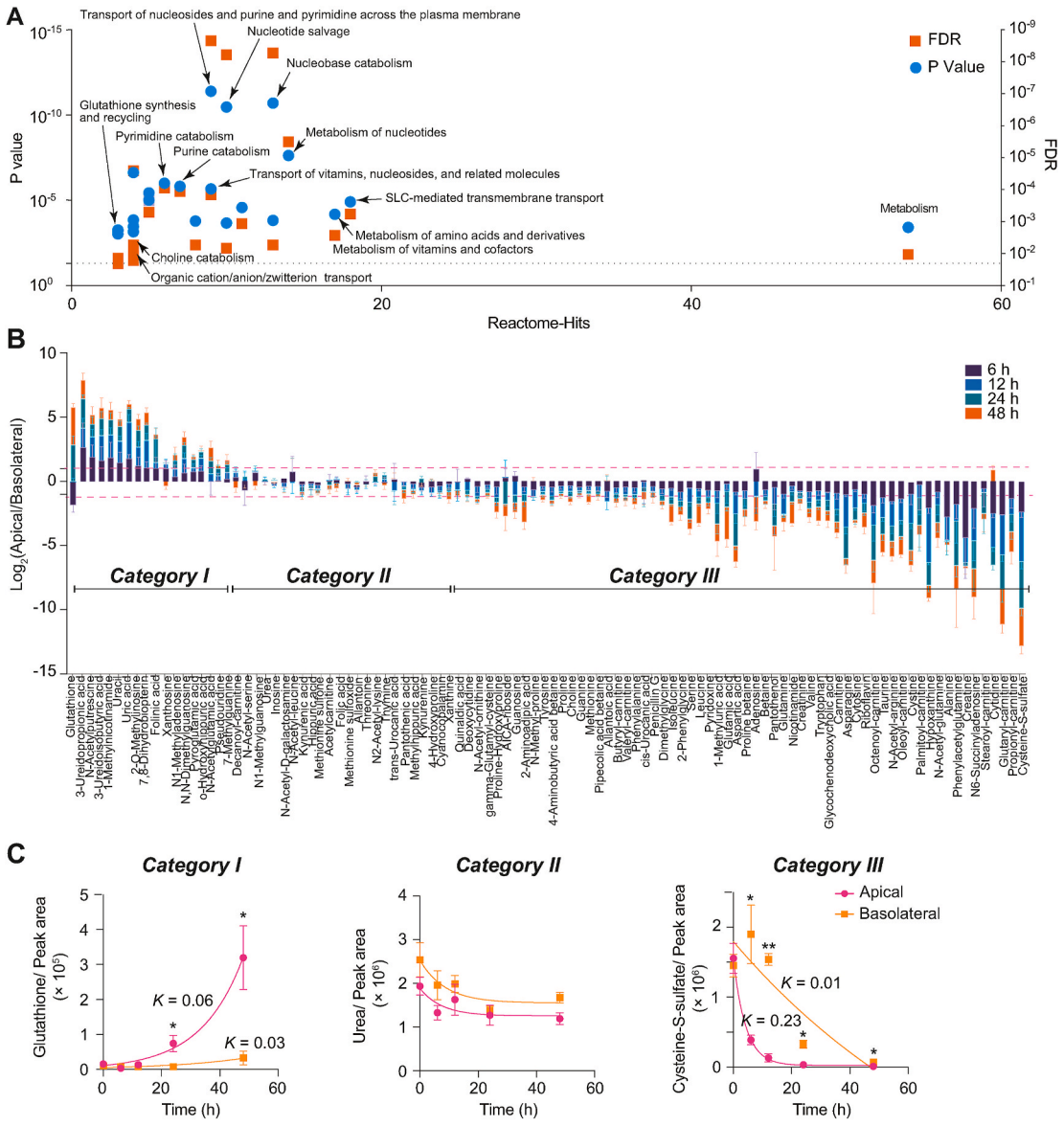

Fig. 4. The determination of biological pathways as well as the transportation tendencies of extracellular metabolites. (A) Metabolic pathway analysis based on the detection of metabolites found in both the apical and basolateral sides of the corneal epithelial barrier show the prediction hits and statistical significance of *P*-values and false discovery ratio (FDR) values. (B) The ratio folds change (log_2 apical/basolateral, pink line indicates ±2-fold difference) of metabolites abundances normalized by 0 time point. (C) Representative examples of the metabolites in Categories I, II, and III. Peak areas were corrected by the channels volume. Data are presented in triplicates as means ± S.E.M. The secretion and depletion rate (*K*) was obtained using exponential (Malthusian) growth and one phase decay models. *P-value <0.05, **P-value <0.001.

cannot be casually conducted in vivo due to their invasive manner. Moreover, the current in vitro models of the human corneal epithelium are both biologically and biomechanically different from the human cornea which albeit the need to more advanced experimental tools for the accurate determination of metabolites activities.

In this study we have utilized a corneal epithelium on a chip, CEpOC, along with an untargeted metabolomic workflow for the accurate determination of micro-scaled extracellular metabolites. The microfluidic device consists of four sets of upper and lower channels separated by a clear polyethylene terephthalate (PET) porous membrane. The porous membrane allows the culturing of corneal epithelial cells with distinguished apical and basal sides, as well as exchange of molecules through the pores. The upper and lower layers are made of polydimethylsiloxane (PDMS), which allows high diffusion of gases, thereby providing a suitable environment for cell growth and expansion (Kamei et al., 2016). This device allowed the application of eye blinking-like shear stress stimulus on the cultured corneal cells as well as the simulation of the aqueous humor flow (Abdalkader and Kamei, 2020). Thus, unlike conventional cell-culture transwell inserts, this chip provides physiologically better conditions for cultured corneal epithelial cells by retaining their normal functions.

We used human corneal epithelial cells (HCE-T), since these cells stably express sufficient metabolic enzymes (Kölln and Reichl, 2012a) and transmembrane transporters (Becker et al., 2007), and have long been used for ocular drug development (Reichl, 2008). Previously we reported that HCE-T can form an intact barrier in the microfluidic device after 7 days of cell culture. Based on this protocol, cells were inoculated in the upper channel having a surface area of 0.23 cm^2, which is five-times smaller than that of the human cornea (human cornea, 1.32 cm^3). Molecule exchange across the corneal epithelial barrier formed on the porous membrane is facilitated by the transporting activities of the cultured corneal epithelial cells. HCE-T cells cultured on a chip

expressed both ZO-1 and F-actin proteins on the apical cellular surface, as in natural corneal epithelial cells (Sugrue and Zieske, 1997; Yamaguchi and Takezawa, 2018), indicating their ability to form an intact and functional corneal epithelial barrier. Moreover, the expression of CK-12 and P-gp also known as multidrug-resistance protein 1; MDR1, (Fig. 1D), indicated CEpOC ability to form an intact and functional corneal epithelial barrier.

Previous studies indicated that some SLC transporters were expressed in the corneal epithelium, mainly SLC22 family members [also known as organic zwitterions/cation transporters (OCTNs) and organic anion transporters (OATs)], owing to their role in the transportation of cationic and anionic drugs (Xiang et al., 2009). Our results as shown in Fig. 2 indicated that more SLC subfamilies that are responsible for trafficking of neutral amino acids (SLC38), copper (SLC31), nucleosides (SLC29), monocarboxylate (SLC16), heteromeric amino acids (SLC7), and sugar alcohol (SLC2) were expressed in HCE-T cells. In fact, the expression of ABC transporters, mainly ABCC1-C2, ABCG2, and ABCB1, which are known for their activities in the efflux of molecules into the extracellular space, has already been reported in HCE-T cells (Becker et al., 2007; Vellonen et al., 2010). In addition, we found that the corneal epithelial cells expressed ABCC4/C5/C16 (cyclic nucleotide transport) as well as other subgroups such as ABCFD1/D4 (fatty acid transport) (Alexander et al., 2015). Although ABCF1 expression was clearly observed, it might not function as a transporter because of the lack of a putative transmembrane domain (Zhang, 2007). Taken together, these results indicate the ability of our CEpOC model to express major transporters that can mediate the transportation of different nutrients as well as drugs.

To perform metabolomic analysis by using CEpOC, we conducted the procedures shown in Fig. 3A. Cells were maintained under the same culture conditions to monitor the consumption of nutrients and secretion of metabolites (Fig. 3A and Table S3–S5). Using untargeted LC-MS workflow we could annotate 104 metabolites. In PCA graphs samples were clustered by all groups (Apical, Basal) indicating systematic metabolite shifts (Fig. 3D and Fig. S3). Calcein AM staining of cells in different microfluidic channels after 48 h indicated that no cellular damage occurred during the 48 h of the sample collection for metabolomics analysis (Fig. 3B and C).

In polarized epithelial barriers, the uptake or secretion of metabolites is known to vary between the apical and basolateral sides. To discriminate these activities, we normalized metabolites by 0 h time point peak areas (considered as control) and then used the $\log_2$ ratio of the normalized values of the apical sides divided by those of the basolateral sides as an indicator of the transportation tendency of metabolite secretion (fold change, $\geq$2; Fig. 4B).

As shown in Fig. 4B in Category I, glutathione (GSH), an endogenous thiol-containing tripeptide, and uric acid derivatives were notably secreted. Both of these metabolites are naturally secreted into human tears and aqueous humor. They are the most abundant antioxidant for their role in cell detoxification of the cornea and conjunctiva (Chen et al., 2009; Ganea and Harding, 2006; Gukasyan et al., 2007). The transepithelial transportation of GSH through the apical sides has been reported to be facilitated by ABC transporter family members (ABCC1/C2/C3/C4/C5) (Bai et al., 2004; Borst et al., 2007; Cole and Deeley, 2006; Gukasyan et al., 2002; Minich et al., 2006). According to the quantitative RT-PCR results shown in Fig. 2, the HCE-T cells in the CEpOC expressed ABCC1, ABCC4, and ABCC5, and the former two were expressed on the apical side, and the latter was strongly expressed at the basolateral side (Vellonen et al., 2010). The presence of more efflux transporters in the apical slide of the barrier suggested that the secretion of GSH secretion was greater on the apical side of the barrier ($K = 0.06$ h^{-1}) than on the basolateral sides ($K = 0.03$ h^{-1}; Fig. 4C). Moreover, a rapid onset of uric acid secretion was noted on the apical sides at 24 h (Fig. 4A). Uric acid and its derivatives are also reported to be effluxed by ABCC4 and ABCG2, which are mainly expressed on the apical sides, as well as SLC22A11/A12 organic anion transporters, which are distributed in both apical and basolateral directions (Nigam et al., 2015; So and Thorens, 2010). Considering the notable expression of ABCC4 and ABCG2 and basal activities of SLC22A11/A12 in the CEpOC, the secretion kinetics of uric acid might have been regulated by both apical-and basal-related transporters. Taken together, these results indicated that our model could simulate the in vivo secretion of important extracellular metabolites.

Notably, in spite of the slight changes in metabolites activities in Category II, the interpretation of fold change data does not necessarily suggest that these metabolites are not regulated by cellular transporters such as vitamin and amino acid transporters (Fig. 4B). Urea levels slightly decreased, but the depletion rate was not considerably different between the apical and basal sides (Fig. 4C).

The transportation of amino acids and their derivatives (e.g., cysteine-*S*-sulfate) is known to be mediated by the SLC7 family of transporters (Jäger et al., 2009), whereas that of nucleoside-related metabolites such as hypoxanthine has been reported to be mediated by nucleoside transporters (e.g., SLC29A2 and SLC29A3) on the apical side of the cornea. Interestingly, RT-PCR results indicated the expression of a wide range of SLC7 family members (SLC7A5/A6/A7/A8/A11) as well as of SLC9A1/A2, which is responsible for the quicker depletion of Category III metabolites, on the apical side of the corneal epithelial barrier.

Remarkably, carnitine and its ester derivatives (glutaryl-/octenoyl-/propionyl-/oleoyl-/palmitoyl-carnitine) were notably depleted on the apical sides of the barrier (Fig. 4B). The carnitine shuttle is an essential process for delivering fatty acids into the mitochondria for the initiation of b-oxidation and the tricarboxylic acid cycle, eventually boosting cell energy (Longo et al., 2016). The uptake and recycling of carnitine are widely performed by SLC22 transporters (apical direction) (Garrett et al., 2008; Xu et al., 2010). We showed an essential process of fatty acid transport through the carnitine shuttling system by detecting a wide range of intermediate ester derivatives with different lengths of fatty acids (Giesbertz et al., 2015). The efflux of acylcarnitines from the mitochondria into the cytosol and further into the extracellular space is important during impaired fatty acid oxidation to stop the accumulation of toxic acyl-CoA in the mitochondria; however, the mechanism beyond their release is not yet known (Ventura et al., 1998).

Currently our CEpOC contain two layers of corneal epithelial cells. Incorporation of additional cell types present in the cornea will provide a more comprehensive approach for studying metabolism and drug transportation in the human cornea. However, CEpOC allows investigation of metabolite activities between the apical and the basolateral side, where anatomically layered stromal and corneal endothelial cells exist in the in vivo structure of the human cornea. Such activities have been reported to facilitate the transportation of different nutrients (e.g., glucose) between the corneal epithelium and endothelium (Diecke et al., 2007; Williams and Watsky, 2004). Our CEpOC platform can also be used for the elucidation of metabolite molecular signaling among different cells.

5. Conclusion

In this study, we introduce corneal epithelium on a chip that enables spatiotemporal collection and analysis of extracellular metabolites. The spatiotemporal determination of extracellular metabolites allows the investigation of important intracellular biological activities across the corneal epithelium, such as metabolite secretion and depletion. In addition, our approach facilitates the noninvasive prediction of the active transportation sites of extracellular metabolites without requiring additional chemical substrates for a specific transporter. We found that antioxidants such as glutathione and uric acid could be secreted from the corneal cells in the CEpOC recapitulating similar vivo secretion conditions. These metabolites are attractive biomarkers for measuring the stress level in cells and can thus be considered as indicators of cell toxicity during the obstruction of corneal homeostasis. Therefore,

considering the nascent level of these studies, our approach can provide valuable methodology for further investigation of secretion and transportation of exogenous and endogenous compounds in future.

Disclosure

The authors declare that there is no conflict of interests.

Authors contributions

R.A and R.C. conceptualized and contributed equally to the project. R.A managed the project, designed and performed microfluidic, biological experiments, analyzed/interpreted data, visualized data, and wrote the manuscript. R.C. designed and performed untargeted metabolomic LC-MS analysis experiments, analyzed/interpreted data, and edited the manuscript. K.K, contributed to data interpretation, data visualization and edited the manuscript. C.W contributed to data interpretation and edited the manuscript. All authors critically reviewed the manuscript and agreed on the publication.

Acknowledgments

Funding was generously provided by the Japan Society for the Promotion of Science (JSPS; 20K20168 to R.A, 17H02083, 18KK0306 and 19H02572 to K.K), Japan Agency for Medical Research and Development (AMED; 17937667) to K.K, Kyoto University GAP fund program (207010) to R.A, and LiaoNing Revitalization Talents Program (XLYC1902061) to K.K. WPI-iCeMS is supported by the World Premier International Research Centre Initiative (WPI), MEXT, Japan. We acknowledge the support from the Gunma University Initiative for Advanced Research (GIAR). We also acknowledge the iCeMS analysis center for providing the imaging facility.

Appendix A. Supplementary data

Supplementary data related to this article can be found at https://doi.org/10.1016/j.exer.2021.108646.

References

Abdalkader, R., Chaleckis, R., Meister, I., Zhang, P., Weelock, C.E., Kamei, K., 2020. Untargeted LC-MS metabolomics for the analysis of micro-scaled extracellular metabolites from *hepatocytes*. Anal. Sci. https://doi.org/10.2116/analsci.20N032 advpub.

Abdalkader, R., Kamei, K.-I., 2020. Multi-corneal barrier-on-a-chip to recapitulate eye blinking shear stress forces. Lab Chip 20, 1410–1417. https://doi.org/10.1039/C9LC01256G.

Alexander, S.P.H., Kelly, E., Marrion, N., Peters, J.A., Benson, H.E., Faccenda, E., Pawson, A.J., Sharman, J.L., Southan, C., Davies, J.A., 2015. The concise guide to PHARMACOLOGY 2015/16: transporters. Br. J. Pharmacol. 172, 6110–6202. https://doi.org/10.1111/bph.13355.

Argikar, U.A., Dumouchel, J.L., Kramlinger, V.M., Cirello, A.L., Gunduz, M., Dunne, C.E., Sohal, B., 2017. Do we need to study metabolism and distribution in the eye: why, when, and are we there yet? J. Pharm. Sci. 106, 2276–2281. https://doi.org/10.1016/j.xphs.2017.03.008.

Bai, J., Lai, L., Yeo, H.C., Goh, B.C., Tan, T.M.C., 2004. Multidrug resistance protein 4 (MRP4/ABCC4) mediates efflux of bimane-glutathione. Int. J. Biochem. Cell Biol. 36, 247–257. https://doi.org/10.1016/S1357-2725(03)00236-X.

Becker, U., Ehrhardt, C., Daum, N., Baldes, C., Schaefer, U.F., Ruprecht, K.W., Kim, K.-J., Lehr, C.-M., 2007. Expression of ABC-transporters in human corneal tissue and the transformed cell line, HCE-T. J. Ocul. Pharmacol. Therapeut. 23, 172–181. https://doi.org/10.1089/jop.2006.0095.

Bennet, D., Estlack, Z., Reid, T., Kim, J., 2018. A microengineered human corneal epithelium-on-a-chip for eye drops mass transport evaluation. Lab Chip 18, 1539–1551. https://doi.org/10.1039/C8LC00158H.

Bhatia, S.N., Ingber, D.E., 2014. Microfluidic organs-on-chips. Nat. Biotechnol. 32, 760–772. https://doi.org/10.1038/nbt.2989.

Borst, P., de Wolf, C., van de Wetering, K., 2007. Multidrug resistance-associated proteins 3, 4, and 5. Pflügers Arch. - Eur. J. Physiol. 453, 661–673. https://doi.org/10.1007/s00424-006-0054-9.

Bovard, D., Sandoz, A., Luettich, K., Frentzel, S., Iskandar, A., Marescotti, D., Trivedi, K., Guedj, E., Dutertre, Q., Peitsch, M.C., Hoeng, J., 2018. A lung/liver-on-a-chip platform for acute and chronic toxicity studies. Lab Chip 18, 3814–3829. https://doi.org/10.1039/C8LC01029C.

Broadhurst, D., Goodacre, R., Reinke, S.N., Kuligowski, J., Wilson, I.D., Lewis, M.R., Dunn, W.B., 2018. Guidelines and considerations for the use of system suitability and quality control samples in mass spectrometry assays applied in untargeted clinical metabolomic studies. Metabolomics 14, 72. https://doi.org/10.1007/s11306-018-1367-3.

Čejková, J., Ardan, T., Filipec, M., Midelfart, A., 2002. Xanthine oxidoreductase and xanthine oxidase in human cornea. Histol. Histopathol. https://doi.org/10.14670/HH-17.755.

Čejková, J., Vejražka, M., Pláteník, J., Štípek, S., 2004. Age-related changes in superoxide dismutase, glutathione peroxidase, catalase and xanthine oxidoreductase/xanthine oxidase activities in the rabbit cornea. Exp. Gerontol. 39, 1537–1543. https://doi.org/10.1016/j.exger.2004.08.006.

Chaleckis, R., Naz, S., Meister, I., Wheelock, C.E., Clifton, N.J., 2018. LC-MS-Based metabolomics of biofluids using all-ion fragmentation (AIF) acquisition. In: Methods in Molecular Biology, pp. 45–58. https://doi.org/10.1007/978-1-4939-7592-1_3. United States.

Chambers, M.C., Maclean, B., Burke, R., Amodei, D., Ruderman, D.L., Neumann, S., Gatto, L., Fischer, B., Pratt, B., Egertson, J., Hoff, K., Kessner, D., Tasman, N., Shulman, N., Frewen, B., Baker, T.A., Brusniak, M.-Y., Paulse, C., Creasy, D., Flashner, L., Kani, K., Moulding, C., Seymour, S.L., Nuwaysir, L.M., Lefebvre, B., Kuhlmann, F., Roark, J., Rainer, P., Detlev, S., Hemenway, T., Huhmer, A., Langridge, J., Connolly, B., Chadick, T., Holly, K., Eckels, J., Deutsch, E.W., Moritz, R.L., Katz, J.E., Agus, D.B., MacCoss, M., Tabb, D.L., Mallick, P., 2012. A cross-platform toolkit for mass spectrometry and proteomics. Nat. Biotechnol. 30, 918–920. https://doi.org/10.1038/nbt.2377.

Chen, Y., Mehta, G., Vasiliou, V., 2009. Antioxidant defenses in the ocular surface. Ocul. Surf. 7, 176–185. https://doi.org/10.1016/S1542-0124(12)70185-4.

Chong, J., Soufan, O., Li, C., Caraus, I., Li, S., Bourque, G., Wishart, D.S., Xia, J., 2018. MetaboAnalyst 4.0: towards more transparent and integrative metabolomics analysis. Nucleic Acids Res. 46, W486–W494. https://doi.org/10.1093/nar/gky310.

Cole, S.P.C., Deeley, R.G., 2006. Transport of glutathione and glutathione conjugates by MRP1. Trends Pharmacol. Sci. 27, 438–446. https://doi.org/10.1016/j.tips.2006.06.008.

Dahlin, A., Geier, E., Stocker, S.L., Cropp, C.D., Grigorenko, E., Bloomer, M., Siegenthaler, J., Xu, L., Basile, A.S., Tang-Liu, D.D.S., Giacomini, K.M., 2013. Gene expression profiling of transporters in the solute carrier and ATP-binding cassette superfamilies in human eye substructures. Mol. Pharm. 10, 650–663. https://doi.org/10.1021/mp300429e.

Diecke, F.P.J., Ma, L., Iserovich, P., Fischbarg, J., 2007. Corneal endothelium transports fluid in the absence of net solute transport. Biochim. Biophys. Acta Biomembr. 1768, 2043–2048. https://doi.org/10.1016/j.bbamem.2007.05.020.

Fabregat, A., Sidiropoulos, K., Viteri, G., Marin-Garcia, P., Ping, P., Stein, L., D'Eustachio, P., Hermjakob, H., 2018. Reactome diagram viewer: data structures and strategies to boost performance. Bioinformatics 34, 1208–1214. https://doi.org/10.1093/bioinformatics/btx752.

Ganea, E., Harding, J.J., 2006. Glutathione-related enzymes and the eye. Curr. Eye Res. 31, 1–11. https://doi.org/10.1080/02713680500477347.

Garrett, Q., Xu, S., Simmons, P.A., Vehige, J., Flanagan, J.L., Willcox, M.D., 2008. Expression and localization of carnitine/organic cation transporter OCTN1 and OCTN2 in ocular epithelium. Investig. Opthalmology Vis. Sci. 49, 4844–4849. https://doi.org/10.1167/iovs.07-1528.

Giesbertz, P., Ecker, J., Haag, A., Spanier, B., Daniel, H., 2015. An LC-MS/MS method to quantify acylcarnitine species including isomeric and odd-numbered forms in plasma and tissues. J. Lipid Res. 56, 2029–2039. https://doi.org/10.1194/jlr.D061721.

Gukasyan, H.J., Kim, K.-J., Lee, V.H.L., Kannan, R., 2007. Glutathione and its transporters in ocular surface defense. Ocul. Surf. 5, 269–279. https://doi.org/10.1016/s1542-0124(12)70093-9.

Gukasyan, H.J., Lee, V.H.L., Kim, K.-J., Kannan, R., 2002. Net glutathione secretion across primary cultured rabbit conjunctival epithelial cell layers. Invest. Ophthalmol. Vis. Sci. 43, 1154–1161.

Haug, K., Cochrane, K., Nainala, V.C., Williams, M., Chang, J., Jayaseelan, K.V., O'Donovan, C., 2020. MetaboLights: a resource evolving in response to the needs of its scientific community. Nucleic Acids Res. 48, D440–D444. https://doi.org/10.1093/nar/gkz1019.

Hornof, M., Toropainen, E., Urtti, A., 2005. Cell culture models of the ocular barriers. Eur. J. Pharm. Biopharm. 60, 207–225. https://doi.org/10.1016/j.ejpb.2005.01.009.

Huh, D., Matthews, B.D., Mammoto, A., Montoya-Zavala, M., Hsin, H.Y., Ingber, D.E., 2010. Reconstituting organ-level lung functions on a chip. Science (80-.) 328, 1662–1668. https://doi.org/10.1126/science.1188302.

Jäger, K., Bönisch, U., Risch, M., Worlitzsch, D., Paulsen, F., 2009. Detection and regulation of cationic amino acid transporters in healthy and diseased ocular surface. Investig. Opthalmology Vis. Sci. 50, 1112. https://doi.org/10.1167/iovs.08-2368.

Jang, K.-J., Otieno, M.A., Ronxhi, J., Lim, H.-K., Ewart, L., Kodella, K.R., Petropolis, D.B., Kulkarni, G., Rubins, J.E., Conegliano, D., Nawroth, J., Simic, D., Lam, W., Singer, M., Barale, E., Singh, B., Sonee, M., Streeter, A.J., Manthey, C., Jones, B., Srivastava, A., Andersson, L.C., Williams, D., Park, H., Barrile, R., Sliz, J., Herland, A., Haney, S., Karalis, K., Ingber, D.E., Hamilton, G.A., 2019. Reproducing human and cross-species drug toxicities using a Liver-Chip. Sci. Transl. Med. 11 https://doi.org/10.1126/scitranslmed.aax5516 eaax5516.

Kamei, K., Koyama, Y., Tokunaga, Y., Mashimo, Y., Yoshioka, M., Fockenberg, C., Mosbergen, R., Korn, O., Wells, C., Chen, Y., 2016. Characterization of phenotypic and transcriptional differences in human pluripotent stem cells under 2D and 3D culture conditions. Adv. Healthc. Mater. 5, 2951–2958. https://doi.org/10.1002/adhm.201600893.

Kamei, K., Mashimo, Y., Koyama, Y., Fockenberg, C., Nakashima, M., Nakajima, M., Li, J., Chen, Y., 2015. 3D printing of soft lithography mold for rapid production of polydimethylsiloxane-based microfluidic devices for cell stimulation with concentration gradients. Biomed. Microdevices 17, 36. https://doi.org/10.1007/s10544-015-9928-y.

Kölln, C., Reichl, S., 2012. mRNA expression of metabolic enzymes in human cornea, corneal cell lines, and hemicornea constructs. J. Ocul. Pharmacol. Therapeut. 28, 271–277. https://doi.org/10.1089/jop.2011.0124.

Larrea, X., De courten, C., Feingold, V., Burger, J., Büchler, P., 2007. Oxygen and glucose distribution after intracorneal lens implantation. Optom. Vis. Sci. 84, 1074–1081. https://doi.org/10.1097/OPX.0b013e31815b9dd6.

Lin, L., Yee, S.W., Kim, R.B., Giacomini, K.M., 2015. SLC transporters as therapeutic targets: emerging opportunities. Nat. Rev. Drug Discov. 14, 543–560. https://doi.org/10.1038/nrd4626.

Longo, N., Frigeni, M., Pasquali, M., 2016. Carnitine transport and fatty acid oxidation. Biochim. Biophys. Acta Mol. Cell Res. 1863, 2422–2435. https://doi.org/10.1016/j.bbamcr.2016.01.023.

McAleer, C.W., Pointon, A., Long, C.J., Brighton, R.L., Wilkin, B.D., Bridges, L.R., Narasimhan Sriram, N., Fabre, K., McDougall, R., Muse, V.P., Mettetal, J.T., Srivastava, A., Williams, D., Schnepper, M.T., Roles, J.L., Shuler, M.L., Hickman, J. J., Ewart, L., 2019. On the potential of in vitro organ-chip models to define temporal pharmacokinetic-pharmacodynamic relationships. Sci. Rep. 9, 9619. https://doi.org/10.1038/s41598-019-45656-4.

McQuin, C., Goodman, A., Chernyshev, V., Kamentsky, L., Cimini, B.A., Karhohs, K.W., Doan, M., Ding, L., Rafelski, S.M., Thirstrup, D., Wiegraebe, W., Singh, S., Becker, T., Caicedo, J.C., Carpenter, A.E., 2018. CellProfiler 3.0: next-generation image processing for biology. PLoS Biol. 16, e2005970 https://doi.org/10.1371/journal.pbio.2005970.

Meister, I., Zhang, P., Sinha, A., Sköld, C.M., Wheelock, Å.M., Izumi, T., Chaleckis, R., Wheelock, C.E., 2021. High-precision automated workflow for urinary untargeted metabolomic epidemiology. Anal. Chem. acs.analchem 1c00203. https://doi.org/10.1021/acs.analchem.1c00203.

Minich, T., Riemer, J., Schulz, J.B., Wielinga, P., Wijnholds, J., Dringen, R., 2006. The multidrug resistance protein 1 (Mrp1), but not Mrp5, mediates export of glutathione and glutathione disulfide from brain astrocytes. J. Neurochem. 97, 373–384. https://doi.org/10.1111/j.1471-4159.2006.03737.x.

Naz, S., Gallart-Ayala, H., Reinke, S.N., Mathon, C., Blankley, R., Chaleckis, R., Wheelock, C.E., 2017. Development of a liquid chromatography–high resolution mass spectrometry metabolomics method with high specificity for metabolite identification using all ion fragmentation acquisition. Anal. Chem. 89, 7933–7942. https://doi.org/10.1021/acs.analchem.7b00925.

Nigam, S.K., Bush, K.T., Martovetsky, G., Ahn, S.-Y., Liu, H.C., Richard, E., Bhatnagar, V., Wu, W., 2015. The organic anion transporter (OAT) family: a systems biology perspective. Physiol. Rev. 95, 83–123. https://doi.org/10.1152/physrev.00025.2013.

Nirmal, J., Singh, S.B., Biswas, N.R., Thavaraj, V., Azad, R.V., Velpandian, T., 2013. Potential pharmacokinetic role of organic cation transporters in modulating the transcorneal penetration of its substrates administered topically. Eye 27, 1196–1203. https://doi.org/10.1038/eye.2013.146.

Rees, D.C., Johnson, E., Lewinson, O., 2009. ABC transporters: the power to change. Nat. Rev. Mol. Cell Biol. 10, 218–227. https://doi.org/10.1038/nrm2646.

Reichl, S., 2008. Cell culture models of the human cornea - a comparative evaluation of their usefulness to determine ocular drug absorption in-vitro. J. Pharm. Pharmacol. 60, 299–307. https://doi.org/10.1211/jpp.60.3.0004.

Rönkkö, S., Vellonen, K.-S., Järvinen, K., Toropainen, E., Urtti, A., 2016. Human corneal cell culture models for drug toxicity studies. Drug Deliv. Transl. Res. 6, 660–675. https://doi.org/10.1007/s13346-016-0330-y.

Seo, J., Huh, D., 2014. A human blinking "Eye-on-a-chip. In: 18th International Conference on Miniaturized Systems for Chemistry and Life Sciences. MicroTAS, 2014.

Sévin, D.C., Fuhrer, T., Zamboni, N., Sauer, U., 2017. Nontargeted in vitro metabolomics for high-throughput identification of novel enzymes in Escherichia coli. Nat. Methods 14, 187–194. https://doi.org/10.1038/nmeth.4103.

So, A., Thorens, B., 2010. Uric acid transport and disease. J. Clin. Invest. 120, 1791–1799. https://doi.org/10.1172/JCI42344.

Sugrue, S.P., Zieske, J.D., 1997. ZO1 in corneal epithelium: association to the zonula occludens and adherens junctions. Exp. Eye Res. https://doi.org/10.1006/exer.1996.0175.

Sumner, L.W., Amberg, A., Barrett, D., Beale, M.H., Beger, R., Daykin, C.A., Fan, T.W.M., Fiehn, O., Goodacre, R., Griffin, J.L., Hankemeier, T., Hardy, N., Harnly, J., Higashi, R., Kopka, J., Lane, A.N., Lindon, J.C., Marriott, P., Nicholls, A.W., Reily, M. D., Thaden, J.J., Viant, M.R., 2007. Proposed minimum reporting standards for chemical analysis. Metabolomics 3, 211–221. https://doi.org/10.1007/s11306-007-0082-2.

Tada, I., Chaleckis, R., Tsugawa, H., Meister, I., Zhang, P., Lazarinis, N., Dahlén, B., Wheelock, C.E., Arita, M., 2020. Correlation-based deconvolution (CorrDec) to generate high-quality MS2 spectra from data-independent acquisition in multisample studies. Anal. Chem. 92, 11310–11317. https://doi.org/10.1021/acs.analchem.0c01980.

Tada, I., Tsugawa, H., Meister, I., Zhang, P., Shu, R., Katsumi, R., Wheelock, C.E., Arita, M., Chaleckis, R., 2019. Creating a reliable mass spectral–retention time library for all ion fragmentation-based metabolomics. Metabolites 9, 251. https://doi.org/10.3390/metabo9110251.

Theodoridis, G.A., Gika, H.G., Wilson, I.D., 2013. LC-MS-Based nontargeted metabolomics. In: Metabolomics in Practice. Wiley-VCH Verlag GmbH & Co. KGaA, Weinheim, Germany, pp. 93–115. https://doi.org/10.1002/9783527655861.ch5.

Tsugawa, H., Cajka, T., Kind, T., Ma, Y., Higgins, B., Ikeda, K., Kanazawa, M., VanderGheynst, J., Fiehn, O., Arita, M., 2015. MS-DIAL: data-independent MS/MS deconvolution for comprehensive metabolome analysis. Nat. Methods 12, 523–526. https://doi.org/10.1038/nmeth.3393.

Vellonen, K.-S., Mannermaa, E., Turner, H., Häkli, M., Mario Wolosin, J., Tervo, T., Honkakoski, P., Urtti, A., 2010. Effluxing ABC transporters in human corneal epithelium. J. Pharm. Sci. 99, 1087–1098. https://doi.org/10.1002/jps.21878.

Ventura, F.V., Ijlst, L., Ruiter, J., Ofman, R., Costa, C.G., Jakobs, C., Duran, M., De Almeida, I.T., Bieber, L.L., Wanders, R.J.A., 1998. Carnitine palmitoyltransferase II specificity towards beta-oxidation intermediates. Evidence for a reverse carnitine cycle in mitochondria. Eur. J. Biochem. 253, 614–618. https://doi.org/10.1046/j.1432-1327.1998.2530614.x.

Williams, K.K., Watsky, M.A., 2004. Bicarbonate promotes dye coupling in the epithelium and endothelium of the rabbit cornea. Curr. Eye Res. 28, 109–120. https://doi.org/10.1076/ceyr.28.2.109.26234.

Xiang, C.D., Batugo, M., Gale, D.C., Zhang, T., Ye, J., Li, C., Zhou, S., Wu, E.Y., Zhang, E. Y., 2009. Characterization of human corneal epithelial cell model as a surrogate for corneal permeability assessment: metabolism and transport. Drug Metab. Dispos. 37, 992–998. https://doi.org/10.1124/dmd.108.026286.

Xu, S., Flanagan, J.L., Simmons, P.A., Vehige, J., Willcox, M.D., Garrett, Q., 2010. Transport of L-carnitine in human corneal and conjunctival epithelial cells. Mol. Vis. 16, 1823–1831.

Yamaguchi, H., Takezawa, T., 2018. Fabrication of a corneal model composed of corneal epithelial and endothelial cells via a collagen vitrigel membrane functioned as an acellular stroma and its application to the corneal permeability test of chemicals. Drug Metab. Dispos. 46, 1684–1691. https://doi.org/10.1124/dmd.118.080820.

Zhang, J.-T., 2007. Use of arrays to investigate the contribution of ATP-binding cassette transporters to drug resistance in cancer chemotherapy and prediction of chemosensitivity. Cell Res. 17, 311–323. https://doi.org/10.1038/cr.2007.15.

Zhang, T., Xiang, C.D., Gale, D., Carreiro, S., Wu, E.Y., Zhang, E.Y., 2008. Drug transporter and cytochrome P450 mRNA expression in human ocular barriers: implications for ocular drug disposition. Drug Metab. Dispos. 36, 1300–1307. https://doi.org/10.1124/dmd.108.021121.